BL-3A/2012G772

GIXD and GISAXS studies of Ni nanoparticle arrays on fluorite surfaces

Sergey M. Suturin[1,*], Vladimir V. Fedorov[1], Alexander M. Korovin[1], Nikolai S. Sokolov[1], Alexey Nashchekin[1], Konstantin M. Pavlov[2], U.P. Chernincov[3] and Masao Tabuchi[4]

[1]Ioffe Physical-Technical Institute, St. Petersburg 194021, Russia
[2]University of New England, NSW 2351, Australia
[3]Petersburg Nuclear Physics Institute, Gatchina 188300, Russia
[4]Synchrotron Radiation Research Center, Nagoya University, Nagoya, Japan

1 Introduction

In recent years intense research efforts have been devoted to the heterostructures with ferro- and antiferromagnetic layers. Particular effects observed in these systems are of great importance as being related to the design of modern high density magnetic media [1]. Ferromagnetic nanoparticles produced by epitaxial growth of Co or Ni on nonmagnetic CaF_2 / Si or antiferromagnetic MnF_2 (NiF_2) / Si surfaces provide a suitable framework to study magnetically ordered nanosystems. Magnetic properties of samples with semi-continuous ferromagnetic layers of Co / MnF_2 have been recently studied by X-ray magnetic circular dichroism [5] to show proximity effects at the ferromagnet-antiferromagnet interface. To gain better understanding of the magnetic interactions in the layer of ferromagnetic nanoparticles (and optionally an antiferromagnetic underlayer) an extended study is underway aimed at replacement of cobalt by a magnetically softer nickel. Both cobalt and nickel are able to establish a commensurate 2:3 epitaxial interface with CaF_2 as long as their lattice parameters 3.52 Å for Ni and 3.54 Å for Co are ~1.5 smaller than the lattice parameter of CaF_2 (5.46 Å). It is well-known that in strained thin films, nanoparticles and nanowires metastable crystal phases are observed quite often. In particular it has been demonstrated in our previous studies [2, 3] that at 500-600°C Co grows on CaF_2(111) predominantly with face-centered cubic (FCC) lattice whereas at normal conditions Co has a hexagonal close packed (HCP) structure. Given a variety of possible crystal structures, it is important to know which one is realized in the particular system. Herein we report grazing incidence small angle X-ray scattering (GISAXS) and grazing incidence X-ray diffraction (GIXD) applied to investigate shape and crystallographic structure of high-temperature stand-alone Ni nanoparticles grown on different CaF_2 faces. A comparison is made to the similar heterosystems with Co nanoparticles.

2 Experiment

Fluorite layers (CaF_2), nickel and cobalt nanoparticles were grown by molecular beam epitaxy (MBE) on silicon substrates. Stand alone metallic nanoparticles were grown at 500-600°C in three major lattice orientations (111, 110 and 001) produced by appropriate choice of Si substrate face and CaF_2 growth parameters. A 0.1 nm low temperature metal seeding layer was used as a precursor to ensure nucleation of regular arrays of nanoparticles with high crystalline quality. The samples were precharacterized in situ by high energy electron diffraction (RHEED).

Grazing incidence X-ray diffraction and grazing incidence small angle X-ray scattering experiments have been carried out at BL3A beamline of Photon Factory (Tsukuba, Japan). The photons of 12 keV were used at a grazing incidence in the range from 0.3 to 5 deg to increase surface sensitivity. Three dimensional reciprocal space mapping in the vicinity of reciprocal space origin (GISAXS) and reciprocal lattice nodes (GIXD) have been carried out by using either HAMAMATSU C4880-22-46F CCD or Pilatus 100K two-dimensional detectors. The mapping technique comprised of taking a dense series of spherical cross-sections through the area of interest in the reciprocal space. Stacking the cross-section images together and reconstructing the intensity distribution in 3D space was done during and after the experiment by means of the software designed by the authors especially for analysis of the 2D data coming from the experiments conducted at BL3A beamline. In addition to this, dedicated macros for *spec* control software have been designed to automate taking series of 2D images while moving along the designated path in the reciprocal space, to perform optimal choice of the image acquisition parameters and to keep track of the these parameters. The analyzing software utilizes UB-matrix formalism [4] to translate (i, j) pixel coordinates in the image to (q_x, q_y, q_z) coordinates in the reciprocal space. The reconstructed 3D intensity distribution can be conveniently analyzed by plotting linear profiles, 2D cross-sections and projections. The described reciprocal node mapping technique proves highly useful when the objects under study are confined in dimensions or have certain types of defects of the crystal structure. This technique has been so far successfully applied by the authors to the investigation of a number of epitaxial nanoscale heterostructures at BL3A beamline. The results obtained for Co / CaF_2 nanoparticles were presented in Refs. 3 and 4, in the

present paper nickel nanoparticles are discussed and compared to the cobalt nanoparticles, other findings related to the fluoride insulating and antiferromagnetic layers will be described elsewhere.

3 Results and Discussion

Crystal structure and shaping tendency during epitaxial growth of Ni on fluorides was investigated on the samples with nickel nanoparticles grown on CaF_2 at high temperature. Figure 1 shows typical surface morphology measured by scanning electron microscopy (SEM) of Ni / CaF_2 / Si samples with 20 nm nickel coverage. Stand-alone islands grow with island-to-island separation approximately equal to island diameter (liquid-type coalescense) and have hexagonal shape on CaF_2 (111) surface, distorted hexagonal shape on CaF_2 (110) surface and square shape on CaF_2 (001) surface. The measured Ni topography is similar to what was previously reported for cobalt grown on CaF_2 [3]. Complimentary to the SEM images giving a clue to how the nanoparticles are oriented with respect to the substrate, GISAXS was used to have insight into the 3D shape of the nanoparticles.

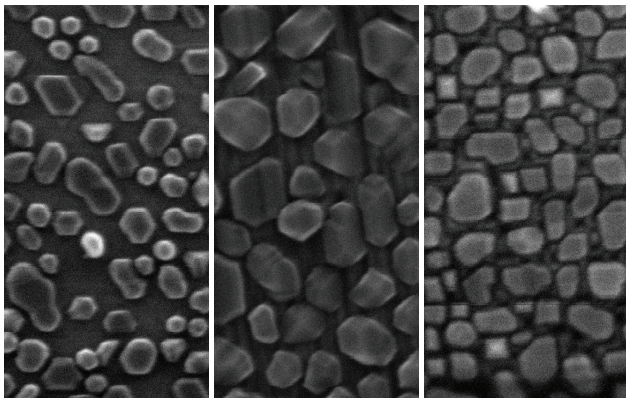

a b c

Fig. 1: SEM images of the 20 nm nickel coverage carried out at 600°C onto CaF_2 (111) (a), CaF_2 (110) (b) and CaF_2 (110) surfaces. SEM image size 300 nm × 600 nm.

During GISAXS measurements the full 360° range of sample rotation around the surface normal (φ) have been investigated. The angle of incidence was kept at about 0.2-0.3°. It has been demonstrated that Ni nanoparticles are facetted with (111) and (001) crystallographic surfaces similar to their cobalt counterparts. Presented in Fig. 2 are intensity distributions in (q_z, q_x) plane reconstructed from a φ-series of GISAXS patterns. During sample rotation around the surface normal the streaks appeared only when the beam got parallel to either (111) or (001) facets. A single GISAXS image that is a spherical cross-section of reciprocal space can grab only part of the streak as the latter lies in the plane perpendicular to the sample surface. Presented here are (q_x, q_z) projections that were compiled from φ-series of images and therefore show full length of the streaks. Appearing of streaks at particular φ values implies that from the point of view of shape the nickel islands are strictly oriented by the underlying CaF_2 layer. As confirmed by electron and X-ray diffraction measurement this holds true also from the point of view of lattice structure - the crystal axes of nickel are cooriented with the crystal axes of CaF_2. The only exception is the limited amount of islands with twinned lattice. An illustration to this is the faint symmetrically mirrored (111) streak observed for Ni(111) islands. The twinned islands are also recognizable on the SEM image in Fig. 1a.

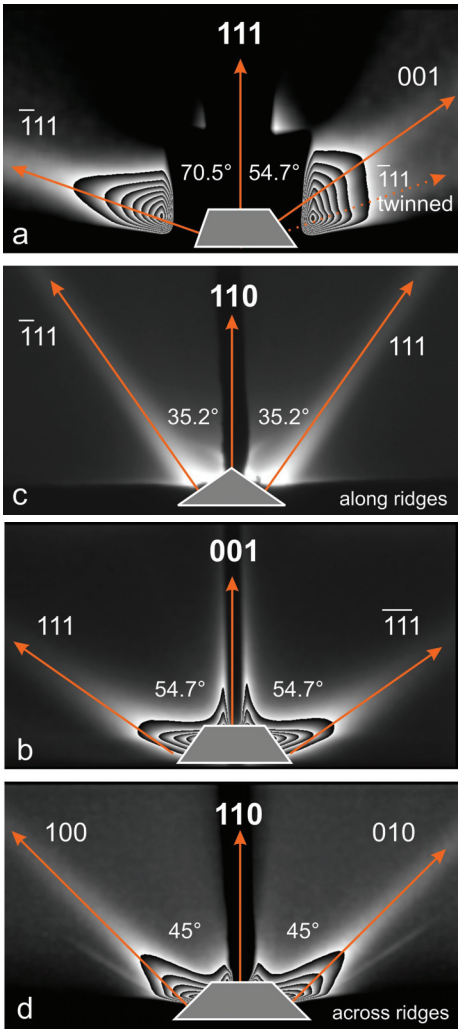

Fig. 2: Facet streaks in (q_x, q_z) intensity distributions obtained from φ-series of GISAXS patterns measured for Ni nanoparticles on CaF_2 (111) (a), CaF_2 (001) (b) and CaF_2 (110) (c, d) surfaces.

For a particle having a cubic lattice there must exist eight {111} facets and six {001} ones. Depending on the orientation different combinations of facets become observable by GISAXS (actually only those that have the facet normal lying above the horizon). By analyzing GISAXS patterns one can conclude that all the observable facets are actually observed which reveals a general rule reading that independent of the island orientation it tends to be facetted by planes belonging to {111} and {001} families. It must be noted that using GISAXS for investigating the facet streaks is important as this tool is not sensitive to the crystal lattice imperfections. As was

shown in our previous works [2, 3] it is important to distinguish between the facet streaks and stacking fault streaks especially when their location in the reciprocal space coincides.

Crystal lattice structure of the facetted nickel nanoparticles of three orientations was further investigated by GIXD. The angle of incidence during these measurements was set to 5 deg in compromise between gaining surface sensitivity (higher at low angles) and minimizing the beam footprint as seen by the detector at Bragg conditions (smaller at high angles). Red curve in Fig. 3a shows an intensity profile passing through Ni(11-1) at Q=0.33 and Ni(220) at Q=1.33. Here Q is measured in convenient reciprocal lattice units corresponding to the interplanar distance in [111] direction (d_{111}=2.03 Å). Smaller peaks at Q=0.66 and Q=1.66 are attributed to Ni(002) and Ni(113) of the twinned phase. The proportion between major and minor phases can be estimated as 6-8:1 by comparing the peak heights. The twinning could be also observed by in situ RHEED measurements (not shown).

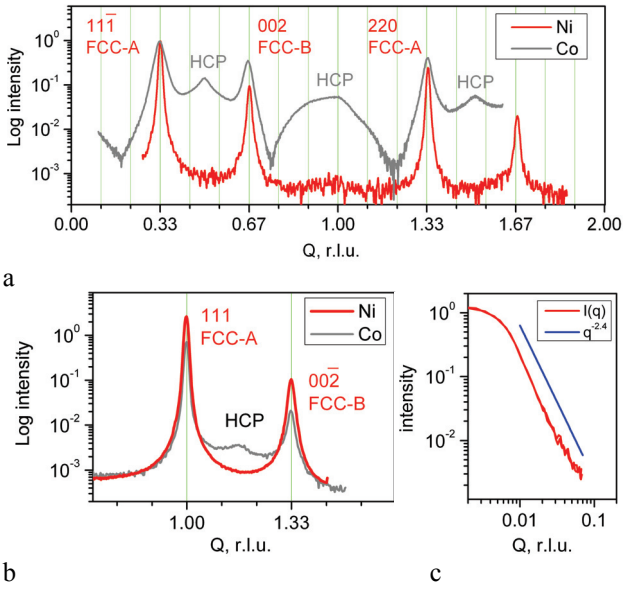

Fig. 3. (A) Intensity profiles along [111] direction passing through (11-1) off-specular reflection measured for Ni(111) 600°C (red) and Co(111) 500°C nanoparticles. (B) Intensity profiles along [11-1] direction passing through (111) off-specular reflection for Ni(110) 600°C (red) and Co(110) 600°C nanoparticles. (C) Simulation of the Ni(11-1) peak slope by the power law $q^{-2.4}$ demonstrating streak like behavior.

It must be noted that all the peaks belong to the face centered cubic (fcc) phase. There are no peaks present at Q=0.5, 1.0 and 1.5 which would be the positions for the hexagonal close packed (HCP) phase. Thus it may be concluded that there is no trace of hexagonal phase in nickel as opposed to cobalt (gray curve in Fig 3a represents a similar profile measured earlier for the 500°C Co nanoparticles). The result is not surprising taking into account that bulk Ni is known to be cubic in the entire temperature range covered during sample fabrication. In opposite, Co is known to be HCP below 450°C and FCC above making the probability of FCC / HCP ratio increasing with temperature. This effect measured for the nanoparticles grown on the CaF_2 (110) microridges is readily seen in Fig. 3b where [11-1] profiles through (111) off-specular reflection are shown for Ni(110) and Co(110) 600°C nanoparticles. Traces of HCP phase are now less prominent in cobalt because of higher growth temperature. Naturally hexagonal phase is never present in nickel. Interestingly peak shapes of Co and Ni reflections look similar (power law) on the outer slopes – left of FCC-A {111} and right of FCC-B {002} peaks. In between the peaks cobalt shows a prominent long streak having maximum at HCP position at Q=0.5 while nickel shows same power law behavior as on the outer slopes.

The intensity decay rate on the peak slopes can be approximated by the power law $q^{-2.4}$ as shown in Fig. 3c. This is a signature of planar truncation of the nickel crystal lattice in the {111} directions. For the case of flat layers, cubic, prismatic or pyramidal islands the q^{-2} power law is expected due to the facets. As the number of facets is increased the exponent in the power law is changing gradually from -2 to -4. For a Ni(111) pyramid truncated with 4 {111} planes and 3 {001} planes the $q^{-2.4}$ behavior seems reasonable and is comparable to what was observed for similar cobalt islands. The FWHM for both major domain and minor (twinned) domain reflections are comparable and correspond to approximately 18 nm of coherently scattering lattice. This is approximately 2/3 of the island height (~30 nm as measured by AFM). The stacking faults are likely formed upon coalescence of separately nucleated islands. Because the nickel lattice constant is 1.5 times smaller than that of CaF_2 there are three possible values for the phase shift between the randomly nucleating Ni islands: 0, $2\pi/3$ and $4\pi/3$. In terms of ABC stacking sequence notation, the coalescence can occur in three ways: ABC-ABC with no fault, CABC-BABC or CABC-BCAB with a fault. This is true if Ni islands are assumed cooriented with the underlying ABC-stacked CaF_2 lattice. Twinning corresponds to the reverse CBACBA sequence and according to the peak height occurs with a probability ~1/6-1/8. Most likely the twinned islands are nucleated on scarce CaF_2 surface defects and grow to the same size as the untwined ones. If the islands are not recrystallized upon coalescence the coherently scattering domain size would give the distance between nucleation sites. However the liquid phase coalescence mechanism of the islands taking place at high growth temperature (similar to [2]) must, to a certain extent, facilitate recrystallization of the islands, reduce the number of stacking faults and increase the size of the coherently scattering domain.

A better perceptible image of reciprocal lattice structure is given by 3D intensity distribution maps measured around Bragg reflections. Figure 4 shows such a map taken around Ni(1-11) reflection for the sample with Ni / CaF_2 (111) nanoparticles. An off-specular

reflection was chosen because it allowed conducting measurements at surface sensitive conditions of 5 deg incidence. The image is reconstructed from two stacks of 2D images: one taken while moving along [1-10] direction and the other along [-111] direction. Distinctly seen on the map is the reciprocal lattice node with bright long streaks emerging in multiple directions. Plotted is the projection along [1 0 -2] as this was found to minimize overlapping between the different streaks.

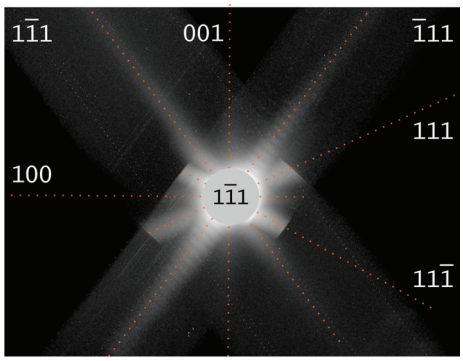

Fig. 4. Three dimensional intensity distribution around Ni(1-11) reflection projected along [1 0 -2] direction. Intensity scale is logarithmic.

The software used to stack the cross-section together is also capable of indexing the observed features. In this particular case four bright streaks are identified as [111]-like and two weaker - as [001]-like. It must be noted that the high frequency intensity oscillations present in the [-111] streak are due to the too big q-steps in scanning and should not be attributed to thickness oscillations or interference fringes. The maps like the one shown are indispensable for detecting and indexing the streaks when their big number makes it impossible to properly resolve them with conventional 1D scanning that utilizes a point detector placed behind a slit. On the particular map of the Ni(1-11) reflection presented in Fig. 4 two steaks are mapped in sufficient Q range: the [1-11] and [-111] ones. From these two the [1-11] one cannot be affected by the stacking order because it is parallel to the stacking direction. The other one is not a radial streak and therefore is stacking order sensitive. Comparable brightness and length of these streaks is an indication of that the stacking faults do not play an important role in forming the streaks in Ni nanoparticles. In other words the coherent domain (the smallest volume with defect-free lattice bounded by the stacking fault planes) almost coincides with the particle body and therefore lattice truncation by the particle facets can be observed in the form of q^{-N} streaks where N slightly exceeds 2. This is opposed to the lattice structure of Co nanoparticles reported earlier [3, 4] where a big number of stacking faults fit inside a single particle thus producing stacking fault streaks that are much longer than the facet streaks. In this case the shape factor of the cobalt particle is considerably smaller than the shape factor of the coherent domain.

Summary

Epitaxial nickel nanoparticles grown onto CaF_2 / Si surfaces with different fluorite orientation have been investigated by from the point of view of size and shape by means of SEM and GISAXS and from the point of view of crystal structure by means of GIXD. Similar to the cobalt nanoparticles studied earlier the nickel islands are facetted with {111} and {100} crystallographic planes. This faceting results in appearance of $q^{-2.4}$ streaks observed during 3D reciprocal space mapping by GISAXS and GIXD. The nickel particles are well oriented by the underlying CaF_2 lattice. A certain proportion of nickel islands exhibit twinned lattice however unlike with cobalt the stacking faults are much lower in density and HCP stacking does never take place. The obtained knowledge related to crystallographic properties of epitaxial ferromagnetic nanoparticles is believed to be important for better understanding of the magnetic properties of these particles grown alone or in conjunction with an antiferromagnet fluoride layer.

Acknowledgement

The study was carried out at PF along the proposal 2012G772. This study has received support from the Russian Government (Megagrant, project 14.V25.31.0025) and the University of Nagoya. The authors wish to acknowledge the BL3A beamline staff for the help in conducting the synchrotron experiments. The SEM measurements have been carried out on the equipment of the Joint Research Center "Material science and characterization in advanced technology" in St. Petersburg.

References

[1] Bae Seongtae,.et al., Spin Valves in Spintronics Applications: Materials, Device Applications, and Electrical, VDM Verlag Dr. Muller, ISBN: 978-3639234794 (2010).

[2] N. S. Sokolov, S. M. Suturin, B. B. Krichevtsov, V. G. Dubrovskii, S. V. Gastev, N. V. Sibirev, D. A. Baranov, V. V. Fedorov, A. A. Sitnikova, A. V. Nashchekin, V. I. Sakharov, I. T. Serenkov, T. Shimada, T. Yanase and M. Tabuchi, *Phys. Rev. B* **87**, 125407 (2013).

[3] S. M. Suturin, V. V. Fedorov, A. M. Korovin, G. A. Valkovskiy, S. G. Konnikov, M. Tabuchi and N. S. Sokolov, *J. Appl. Cryst.* **46** 874 (2013).

[4] Busing, W. R., & Levy, H. a., *Acta Crystallographica*, **22(4)**, 457 (1967).

[5] S M Suturin, V V Fedorov, A G Banshchikov, D A Baranov, K V Koshmak, P Torelli, J Fujii, G Panaccione, K Amemiya, M Sakamaki, T Nakamura, M Tabuchi, L Pasquali and N S Sokolov, *J. Phys.: Condens. Matter* **25** 046002 (2013).

* suturin@mail.ioffe.ru